OPEN

Protopanaxatriol, a novel PPARγ antagonist from *Panax ginseng*, alleviates steatosis in mice

Yu Zhang[1], Lijing Yu[1], Wujie Cai[1], Shengjie Fan[1], Li Feng[1], Guang Ji[2] & Cheng Huang[1]

[1]School of Pharmacy, Shanghai University of Traditional Chinese Medicine, 1200 Cailun Road, Shanghai 201203, China, [2]Institutes of Digestive Disease, Longhua Hospital, Shanghai University of Traditional Chinese Medicine, Shanghai 200032, China.

Obesity is prevalent worldwide, and is highly associated with metabolic disorders, such as insulin resistance, hyperlipidemia and steatosis. Ginseng has been used as food and traditional herbal medicine for the treatment of various metabolic diseases. However, the molecular mechanisms how ginseng and its components participate in the regulation of lipogenesis are still largely unclear. Here, we identified that protopanaxatriol (PPT), a major ginseng constituent, inhibited rosiglitazone-supported adipocyte differentiation of 3T3-L1 cells by repressing the expression of lipogenesis-related gene expression. In high-fat diet-induced obesity (DIO) mice, PPT reduced body weight and serum lipid levels, improved insulin resistance, as well as morphology and lipid accumulation, particular macrovesicular steatosis, in the livers. These effects were confirmed with genetically obese *ob/ob* mice. A reporter gene assay showed that PPT specifically inhibited the transactivity of PPARγ, but not PPAR α, β/δ and LXR α, β. TR-FRET assay revealed that PPT was specifically bound to PPARγ LBD, which was further confirmed by the molecular docking study. Our data demonstrate that PPT is a novel PPARγ antagonist. The inhibition of PPARγ activity could be a promising therapy for obesity and steatosis. Our findings shed new light on the mechanism of ginseng in the treatment of metabolic syndrome.

Peroxisome proliferator-activated receptor (PPAR) γ is a member of the ligand-activated nuclear receptor transcription factor superfamily, which controls lipogenesis, energy and glucose homeostasis, and is also an important drug target for metabolic diseases. PPARγ agonists thiazolidinediones (TZD) are insulin-sensitizing agents, which have promising therapeutic effects on type 2 diabetes. However, hyperactivation of PPARγ by TZD may induce adipose tissue expansion, weight gain and fatty liver in patients and animals[1–3] and adipogenesis *in vitro*[4,5]. On the other hand, heterozygous PPARγ-deficient mice displayed a resistance to high-fat diet-induced insulin resistance and obesity due to adipocyte hypertrophy in C57BL/6 mice[1,6,7]. In addition, hepatic TG content is reduced, and fatty liver is improved in the liver-specific PPARγ deficient mice under *ob/ob* background[8]. Consistent with the findings in PPARγ hetero-knockout mice, several PPARγ antagonists including β-cryptoxanthine and tanshinone IIA have been identified to reduce body and fat weight, and to improve insulin resistance in high-fat diet-induced mice[3,9–11]. The observations above suggest that moderate inhibition of PPARγ activity may reduce the risk for the development of obesity, type 2 diabetes and steatosis, and PPARγ antagonists may be useful for the treatment and prevention of metabolic disorders.

Nonalcoholic fatty liver disease (NAFLD) is associated with obesity and insulin resistance[12,13], and often leads to steatohepatitis, liver fibrosis and cirrhosis[14]. It has been reported that PPARγ signaling is involved in the pathogenesis of hepatic steatosis[15,16]. PPARγ and its targeted genes are specifically up-regulated in the fatty liver induced by a high fat diet[17]. Overexpression of PPARγ in hepatocytes induces the expression of its downstream target gene, which further leads to the development of lipogenic steatosis[15]. Activation of PPARγ by its agonist, rosiglitazone, increases the hepatic triglyceride content, enhances the number and size of hepatic lipid droplets, and triggers pro-steatotic pathways with the aggravation of hepatic lipid accumulation[18]. Treatment of rosiglitazone also results in liver steatosis in *ob/ob* mice[19]. On the other hand, hepatocyte-specific deletion of PPARγ prevents the accumulation of lipids and the development of hepatic steatosis in high-fat diet-fed mice[20,21]. All the evidence above suggests that PPARγ antagonists are potential medications for the therapy of obesity and obesity-related hepatic steatosis.

Ginseng, belonging to the genus *Panax* of the family *Araliaceae*, has been used as food and a tonic herb in the treatment of various diseases including obesity and diabetes in Eastern Asian countries. Ginseng and its con-

stituents ginsenosides play therapeutic roles in *db/db* mice[22], *ob/ob* mice[23], STZ-induced diabetic mice[24,25], and in diabetic patients[26]. Ginseng and ginsenosides can also reduce body weight in high-fat diet-fed mice[27–30] and *ob/ob* mice[28]. These data suggest that ginseng and its constituents are effective for the treatment of metabolic disorders. However, the underlying mechanisms of their therapeutic effects are still largely unclear.

Ginseng contains more than 30 types of saponins (ginsenoside), which are the major active constituents. Protopanaxatriol (PPT), 20(S)-5α-Dammar-24-ene-3β,6α,12β,20-tetrol, is a constituent in the root of *Panax ginseng C. A. Mey*, and a major monoglucoside-metabolized ginsenoside of PPT-type ginsenosides[31], which are the most abundant in *Panax ginseng*[32]. In the present study, we investigated the effects of PPT on metabolic disorders, and found that PPT-treatment could ameliorate obesity, insulin resistance, steatosis and hyperlipidemia in diet-induced obesity (DIO) mice and *ob/ob* mice. Moreover, our data demonstrate that PPT is a novel PPARγ antagonist with moderate binding activity. Thus, our findings provide modern molecular evidence to uncover how ginseng, an old traditional herb medicine, functions for the treatment of metabolic disorders.

Results

PPT inhibits adipocyte differentiation and reduces gene expression in 3T3-L1 cells. Since ginseng has been used for weight-reducing purposes in obese patients, we first asked whether the monoglucoside of ginseng was able to inhibit adipocyte differentiation. A 3T3-L1 adipocyte differentiation model was used in the study, and 20 monoglucosides purified from ginseng were screened to identify their ability to regulate lipogenesis and adipocyte differentiation. The results showed that PPT, Rg1 and Rb1 could suppress the lipogenesis and adipocyte differentiation (Table 1). PPT (Fig. 1a) is a major monoglucoside of Rg1 ginseng ginsenosides following metabolism by intestinal bacteria in humans. Therefore, we focused on PPT in the study due to its lipogenesis inhibitory effect.

Rosiglitazone could strongly promote 3T3-L1 adipocyte differentiation when insulin and dexamethasone were present in the culture medium. We then used rosiglitazone instead of isobutylmethyl xanthine in the induction of 3T3-L1 adipocyte differentiation. We observed that rosiglitazone induced adipocyte differentiation after a 5-day induction period with insulin and dexamethasone, while PPT blocked the lipogenesis induced by rosiglitazone (Fig. 1b). At a concentration of 12.5 μM, PPT slightly inhibited the lipogenesis, and PPT almost completely blocked the lipogenesis in 3T3-L1 adipocyte at 50 μM, suggesting that PPT represses the lipogenesis and adipocyte differentiation induced by rosiglitazone in a dose-dependent manner.

PPARγ and CCAAT-enhancer-binding proteins (C/EBP) are activated at the early stage of 3T3-L1 adipocyte differentiation, which play critical roles in regulating lipogenesis[33,34]. To test whether the observed effect of PPT on the suppression of lipogenesis and adipocyte differentiation was mediated through the PPARγ and C/EBP pathway, the expression of these transcription factors was analyzed in differentiated 3T3-L1 cells at D0 by quantitative real-time PCR. The mRNA levels of PPARγ and C/EBPα were significantly reduced in the differentiated adipocytes treated with PPT (35–40% *vs.* baseline level), whereas the expression of C/EBPβ was not changed (Fig. 1c). The expression of PPARγ and its target genes, adipose fatty acid-binding protein 2 (aP2), cluster of Differentiation 36 (CD36), fatty acid synthase (FAS) and lipoprotein lipase (LPL), was also assessed in D6 differentiated adipocytes. Their expression was markedly decreased (Fig. 1d). Collectively, these results above suggest that PPT inhibits adipocyte differentiation, possibly through repressing the PPARγ signaling.

PPT ameliorates metabolic disorders in high-fat diet-induced obese mice. Previous studies have demonstrated that a moderate reduction of PPARγ activity may reduce the risk for the development of obesity and type 2 diabetes. Since PPT inhibits adipocyte differentiation *in vitro*, we asked whether PPT has the effect on body weight changes in obese C57BL/6 mice. The mice were placed on a high-fat diet for 3-month to induce obesity, and then the obese mice were divided into two groups and fed with HF mixed with 1 g/kg PPT or HF diet alone for 4 weeks. As shown in Fig. 2a, the mice fed with PPT supplementation displayed much lower body weight than control DIO mice at the end of treatment. In addition, electronic scanning microscopy assays showed that the size of adipocytes in WAT of PPT-treated mice was reduced compared to that of the DIO mice (Fig. 2b). PPT treatment did not alter the food intake and the fecal TG in mice (Fig. 2c and 2d). Nevertheless, PPT-treated mice showed a significantly higher body temperature compared to the DIO mice (Fig. 2e), indicating that PPT may enhance the energy expenditure.

Next, we examined whether PPT supplementation would affect blood glucose levels, which commonly correlated to obesity[35,36]. The DIO mice exhibited higher fasting blood glucose levels and impaired glucose tolerance, compared to the chow control mice (Fig. 2f and 2g). Interestingly, PPT treatment markedly reduced fasting blood glucose levels (Fig. 2f). In the i.p. glucose tolerance test experiment, the PPT treatment lowered glucose levels at 30, 60, 90 and 120-min after i.p. injection of 1 g/kg glucose (Fig. 2g). To test the insulin sensitivity in these mice, the insulin tolerance test was conducted. We i.p. injected 0.75 U/kg insulin and measured the blood glucose level at 0, 15, 30, 60, 90 and 120 min intervals. The results showed that the blood glucose levels in the obese mice with PPT supplementation were significant lower at 30, 60, 90 and 120 min, compared to the control DIO mice, indicating that the PPT was able to improve insulin resistance in the DIO mice (Fig. 2h).

Hyperinsulinemia and hyperleptinemia have been shown to correlate with obesity[37,38]. As shown in Fig. 2i and 2j, the HF diet-feeding resulted in an increase in serum insulin and leptin levels in the mice, which were markedly reduced by PPT treatment. Serum adiponectin levels were significantly reduced in the DIO mice when compared to that in chow diet-fed mice. In contrast, PPT supplementation reversed the decrease of adiponectin in DIO mice (Fig. 2k).

Table 1	Effects of gingsen constituents on 3T3-L1 adipocyte differentiation	
compound	**action**
Ginsenoside-Rh1	±
Ginsenoside-Rg2	±
Ginsenoside-CK	X
Ginsenoside-Rc	+
Ginsenoside-Rb3	+
Protopanaxatriol	-
Pseudo ginsenoside-Rf11	±
Pseudo ginsenoside-RT5	±
Ginsenoside-F1	-
Ginsenoside-F2	X
Ginsenoside-Rb2	+
Ginsenoside-Rd	±
Protopanoxadiol	X
Toxifolin	+
Ginsenoside-Rh2	X
Ginsenoside-Ro	+
Ginsenoside-Rb1	±
Ginsenoside-Re	-
Ginsenoside-Rg1	-
Ginsenoside-Rg3	-

Note: +: promotion; -: inhibition; ±: no effect; X: death.
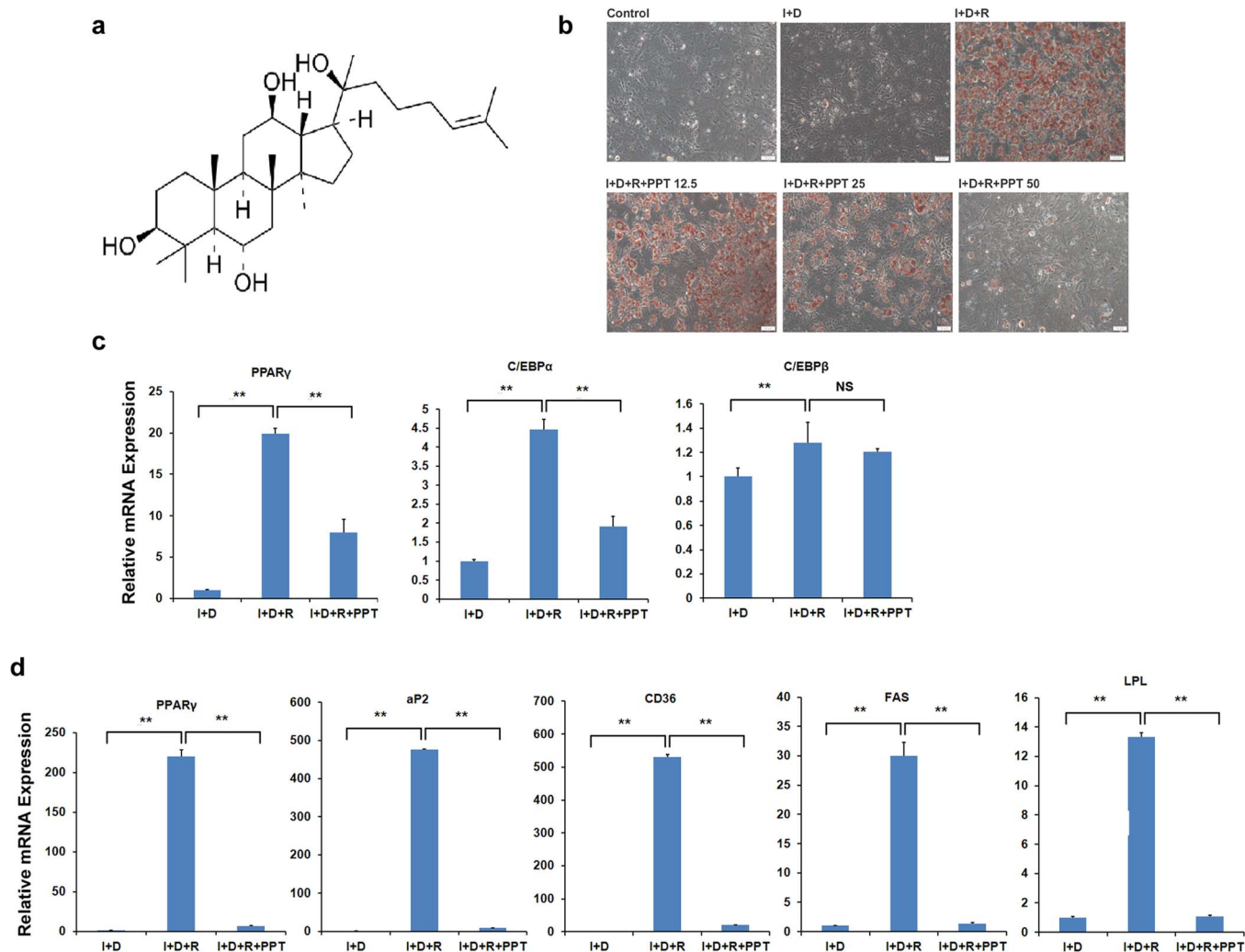
Figure 1 | PPT inhibits 3T3-L1 adipocyte differentiation and adipogenesis related gene expression. (a) Structure of PPT. (b) PPT suppresses 3T3-L1 adipocyte differentiation induced by differentiation medium. Differentiation medium includes 10 μg/ml insulin, 1 μM dexamethasone and 10 μM rosiglitazone. Oil red O staining of 3T3-L1 cells was performed on day 6. PPT was added to the medium at the beginning of induction of 3T3-L1 cells at the indicated concentration. (c) Real-time RT-PCR results of gene expression levels at day 0 in 3T3-L1 adipocyte. Cells were treated with PPT (50 μM) and differentiation medium after confluence for 2 days. (d) Real-time RT-PCR results of gene expression levels at day 6 in 3T3-L1 adipocyte. Cells were treated with PPT (50 μM) and differentiated for 6 days. Control: growth medium. I+D: insulin and dexamethasone. I+D+R: insulin, dexamethasone and rosiglitazone. Mouse beta-actin was used as the control and values representing mRNA of the untreated cells were defined as 1. Data are presented as means ± SEM (n = 3). *$P<0.05$, **$P<0.01$.

Serum chemistry analysis revealed that HF feeding resulted in an increase in the serum levels of TG, TC, LDL-c and HDL-c (Fig. 2l). PPT treatment notably decreased serum TG, TC and LDL-c levels in DIO mice, whereas the HDL-c level remained unchanged (Fig. 2l). Excess free fatty acid (FFA) leads to dyslipidemia and adverse health results of obesity[39]. After 4 week-treatment of PPT, the DIO mice also displayed the lower concentration of FFA (Fig. 2m). The results above indicate that PPT is effective to attenuate HF diet-induced hyperlipidemia *in vivo*.

PPT improves hepatic steatosis and mitochondrial respiratory chain (MRC) level in the liver of DIO mice. Since a high-fat diet induces fatty liver in mice, we further assessed whether PPT could ameliorate the hepatic steatosis by examining the morphology and lipid accumulation in the liver sections. Compared to that of chow diet-fed mice, more fat droplets, microvesicular and macrovesicular were observed in most hepatocytes of the DIO mice (Fig. 3a). In addition, seven of DIO mice displayed grade 3 (>66%) steatosis, and one mouse had grade 2 (33%–66%) steatosis. In 50% to 70%

of hepatocytes, fat was seen mostly as macrovesicular droplets, and 30%–50% of the hepatocytes remained microvesicular steatosis. Biochemistry analysis of hepatic TG content revealed that the amount of TG was significantly increased in DIO mice (Fig. 3b). PPT treatment decreased steatosis by reducing macrovacuolar droplets in liver section. Among PPT-treated mice, seven mice displayed grade 1 (5%–33%) steatosis, and one mouse had grade 2 (33%–66%) steatosis, indicating PPT treatment may prevent or reverse the lipid accumulation in the DIO mice. Also, liver TG concentration was decreased in PPT-treated animals ($P <0.05$ *vs.* DIO mice) (Fig. 3b). However, PPT treatment did not reduce the TC content in the liver of DIO mice (Fig. 3c). Furthermore, PPT lowered the serum AST and ALT levels in DIO mice (Fig. 3d and 3e), indicating that PPT has the capacity to improve liver damage. These results suggest that PPT may prevent lipid accumulation and block the development of hepatic steatosis induced by a high-fat diet in mice.

NAFLD encompasses hepatic steatosis, NASH, fibrosis and cirrhosis. Oxidative stress and MRC level in the mouse liver, which play
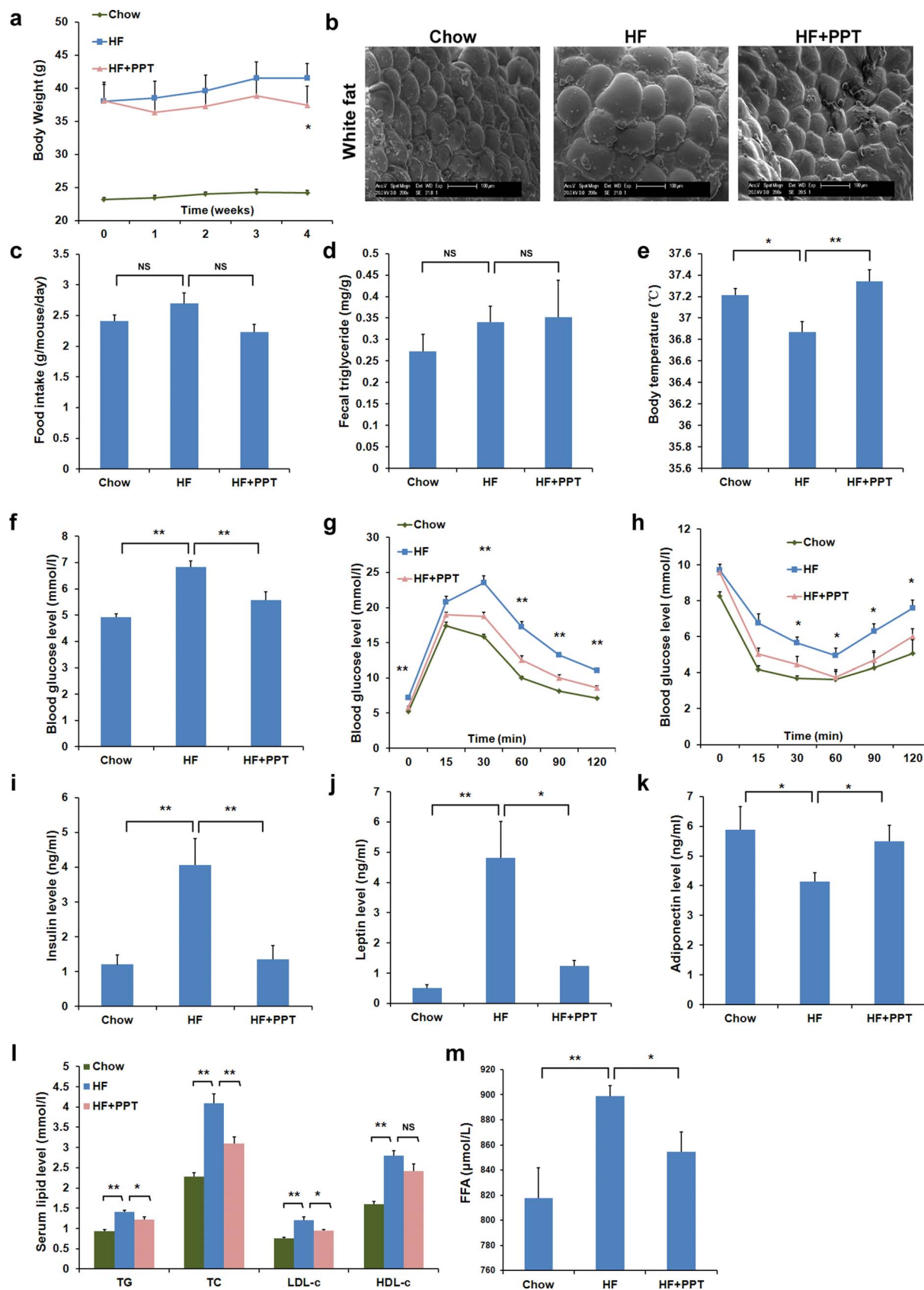
Figure 2 | **PPT ameliorates metabolic disorders in high-fat diet-induced obesity C57BL/6 mice.** (a) Body weight gain. (b) Mass of white adipose tissue. (c) Food intake amount. (d) Fecal triglyceride level. (e) Body temperature. (f) Fasting blood glucose level. (g) Glucose tolerance test (GTT). (h) Insulin tolerance test (ITT). (i) Serum insulin content. (j) Serum leptin content. (k) Serum adiponeciton content. (l) Serum total cholesterol (TC), triglyceride (TG), low-density lipoprotein cholesterol (LDL-c), high-density lipoprotein cholesterol (HDL-c). (m) Free fatty acid (FFA) level. Data are presented as means $\pm$ SEM (n = 8). *$P<0.05$, **$P<0.01$ vs. HF group.
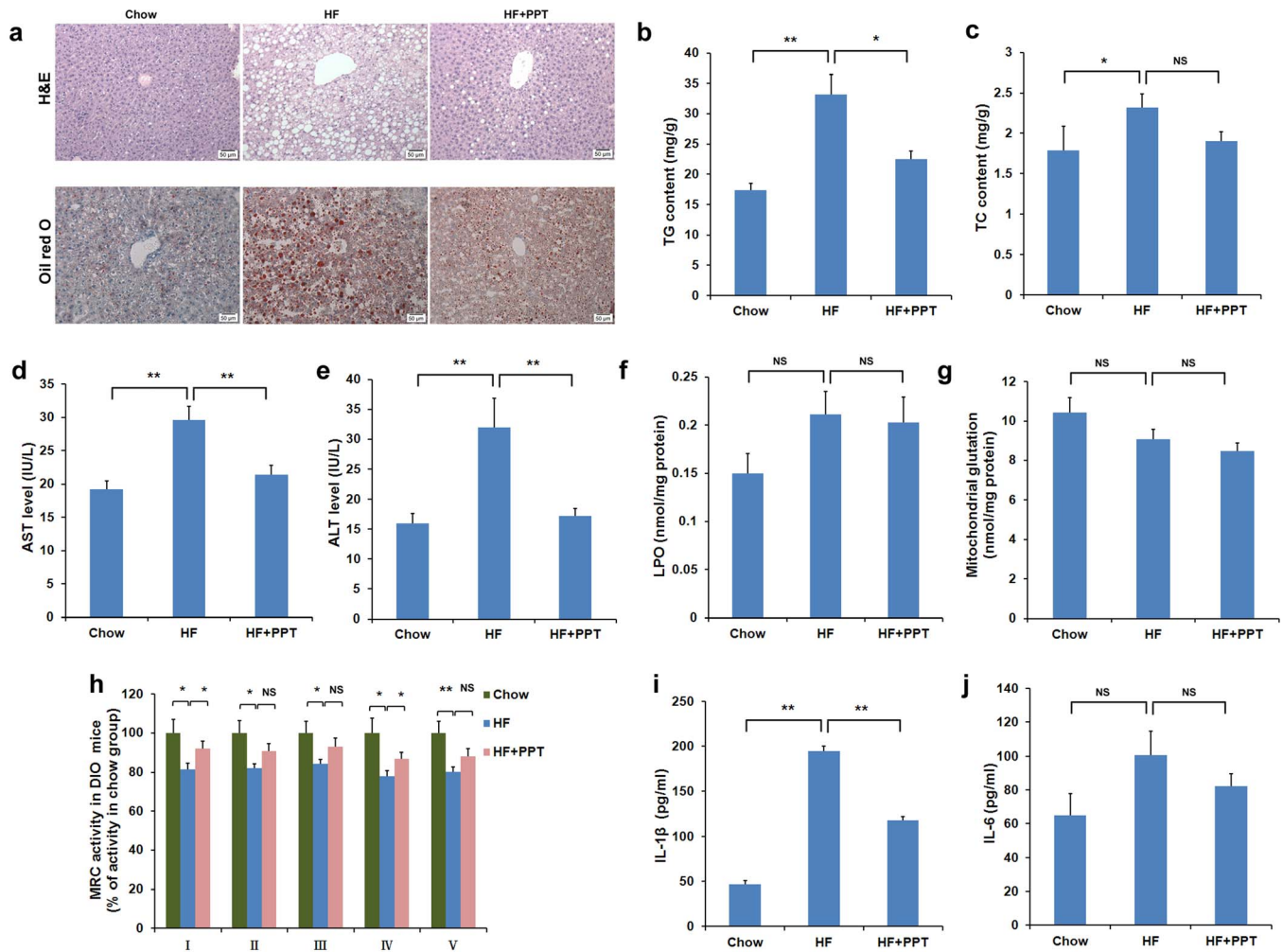
Figure 3 | PPT ameliorates hepatic steatosis in high-fat diet–induced obesity C57BL/6 mice. (a) H&E and Oil red O staining of liver sections (×200). (b) Liver TG level. (c) Liver TC level. (d) Serum AST level. (e) Serum ALT level. (f) Liver LPO (lipid peroxide) content. (g) Liver glutathione content. (h) Mitochondrial respiratory chain level. (i) Serum IL-1β content. (j) Serum IL-6 content. Data are presented as means ± SEM (n = 8). *$P<0.05$, **$P<0.01$vs. HF group.

a key role in the development of NASH, were evaluated. As shown in Fig. 3f and 3g, lipid peroxide levels (Fig. 3f) and glutathione (Fig. 3g) was not remarkably changed in the liver of DIO mice, compared to the chow mice. Nevertheless, PPT intervention did not alter lipid peroxide and glutathione levels (Fig. 3f and 3g). MRC complexes I-V in the liver of the DIO mice were reduced when compared to that of chow diet control mice. The administration of DIO mice with PPT led to a significant increase in MRC complexes I and IV (Fig. 3h).

The further feature of obesity and NAFLD are the abnormalities of inflammatory mediators. Next, the serum interleukin (IL)-1β and IL-6 levels were analyzed. As shown in Fig 3i and 3j, the serum level of IL-1β was remarkably increased in DIO mice. PPT treatment significantly reduced the levels of IL-1β, whereas IL-6 remained unchanged in all groups, suggesting that PPT may ameliorate inflammatory state in DIO mice.

PPT improves metabolic disorders in *ob/ob* mice. To further confirm the effects of PPT on metabolic disorders, the *ob/ob* mouse, which is a model for obesity, insulin resistance, hyperlipidemia and steatosis, was fed with PPT. After treatment with PPT for two weeks, the body weight and food intake of *ob/ob* mice were not altered (Fig. 4a and 4b). However, the fasting blood glucose levels (Fig. 4c) were lower in the PPT-treated group compared to that in control *ob/ob* mice. The glucose tolerance test showed that the blood glucose

levels of the PPT-treated mice were decreased at 60 and 90 min, compared with that of control *ob/ob* mice (Fig. 4d). PPT treatment also significantly attenuated serum TG levels, while serum TC, LDL-c and HDL-c levels remained unchanged (Fig. 4e).

PPT improves hepatic steatosis and MRC level in the liver of *ob/ob* mice. Next, the liver morphology of the mice was examined by using H&E staining. As shown in Fig. 5a, severe macrovesicular steatosis was detected in the liver of the control *ob/ob* mice, and all of them exhibited grade 3 steatosis. Fat was observed as macrovesicular droplets in 80% to 90% of hepatocytes. After PPT treatment, macrovesicular droplets were notably attenuated to 40%–50% of hepatocytes, though only 3 mice were improved to grade 2 steatosis. Oil Red O staining was also performed with the liver sections. Consistently, lipid accumulation was observed in the liver sections of the control *ob/ob* mice, whereas PPT ameliorated the lipid accumulation (Fig. 5a). Liver chemistry analysis showed that TG and TC contents in the control *ob/ob* mice were increased, and PPT treatment reduced TG and TC contents (Fig. 5b and 5c). Consistent with the observations in the DIO mouse model, PPT treatment reduced the levels of AST and ALT, compared with the control *ob/ob* mice (Fig. 5d and 5e). PPT did not change the hepatic lipid peroxide and glutathione levels (Fig. 5f and 5g), whereas PPT increased MRC complex II level in the liver of *ob/ob* mice. (Fig. 5h).

5
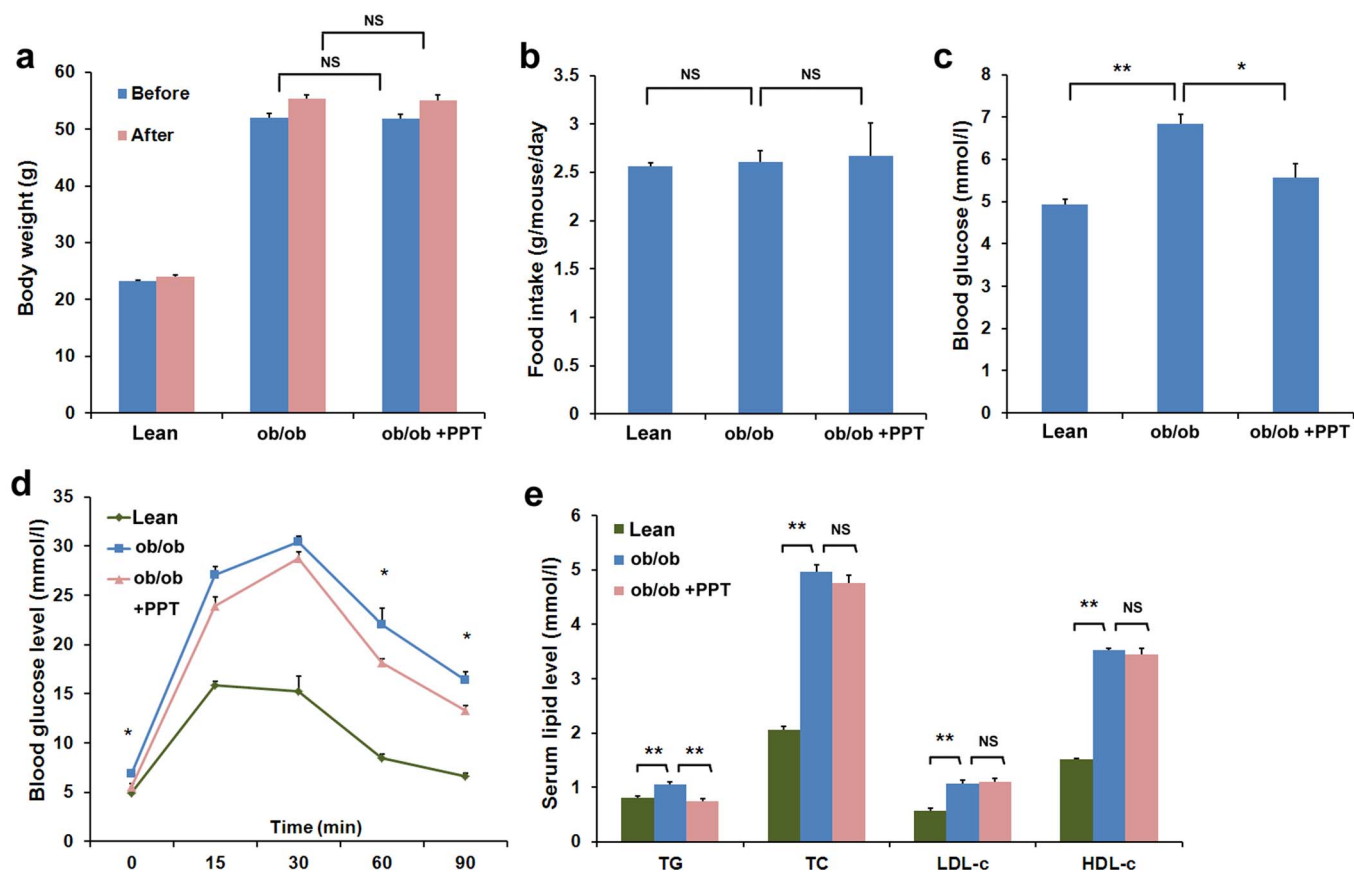
Figure 4 | PPT ameliorates metabolic disorders in *ob/ob* mice. (a) Body weight gain. (b) Food intake amount. (c) Fasting glucose level. (d) Glucose tolerance test (GTT) in *ob/ob* mice. (e) Serum TC, TG, LDL-c, and HDL-c levels. Data are presented as means ± SEM (n = 8). *$P<0.05$, **$P<0.01$ vs. *ob/ob* mice.

PPT is a novel antagonist of PPARγ. Based on the inhibition of adipocyte differentiation, and the modulation of the expression of PPARγ and its downstream genes, we postulated that PPT might target PPARγ directly. To test this hypothesis, HEK293T cells were co-transfected with GAL4-PPARγ ligand-binding domain (LBD) fusion plasmid and a plasmid of the UAS reporter. Rosiglitazone could activate PPARγ transactivity, which was significantly inhibited by PPT (Fig. 6a). In contrast, PPT did not show an inhibitory effect on other nuclear receptors involved in metabolic disorders, such as PPARα and β/σ (Fig. 6b and 6c), LXRα and β (data not shown).

Next, we asked whether PPT is possible a PPARγ antagonist. A competitive binding assay using TR-FRET was performed. Indeed, PPT was able to displace the rosiglitazone from binding to PPARγ at an IC50 value of 11.75 μM (Ki = 4.2 μM). Compared with unlabeled rosiglitazone (Ki= 43 nM), the PPARγ binding affinity of PPT was moderate (Fig. 6d). As expected, PPT showed no binding to PPARα and β/σ (data not shown). Together with the reporter gene assay, these findings indicate that PPT may specifically bind to PPARγ LBD, and function as a PPARγ antagonist.

To further understand the interaction of PPT with PPARγ, the structure of the complex of the PPARγ LBD and PPT was analyzed by molecular docking. The pose ranked first complex with human PPARγ was showed in Fig. 6e. The hydrophobic part of protopanaxatriol, the scaffold of triterpene, interacts with hydrophobic residues, and is the primary reason for protopanaxatriol activity. In addition, there are three different directional H-bonds between hydroxyl at His449, Met364 and Cys285. These H-bonds enhance the binding stability. The specific interaction of PPT with PPAR-gamma LBD is also displayed in a 2D-interaction map (Fig. 6f). Collectively, PPT is a novel antagonist of PPARγ.

PPT regulates metabolic and inflammatory gene expression in vivo. Consistent with the increase of body temperature, the expression of uncoupling protein (UCP)-1, UCP-2 and UCP-3 genes, involved in energy dissipation and adoptive thermogenesis in brown adipose tissue (BAT), was enhanced in the BAT of PPT-treated mice (Fig. 7a). The other adipose tissue involving in the heat production and energy expenditure is beige adipose in WAT. The elevated expression of UCP-1 is a key feature for browning of WAT[40]. Interestingly, PPT treatment increased the expression of UCP-1 in WAT (Fig. 7b). These data suggest that PPT may promote the energy expenditure, which in turn, could also reduce adiposity.

Next, the gene expression profiles of PPARγ and its target genes in the WAT and liver tissue of DIO mice and *ob/ob* mice were analyzed by real time-PCR. In DIO mice, the expression of CD36, FAS and stearoyl-CoA desaturase (SCD)-1 in liver tissue (Fig. 7c) and PPARγ and sterol regulatory element-binding protein (SREBP)-1c in WAT (Fig. 7d) was reduced in the PPT-treated mice. In addition, in *ob/ob* mice the mRNA levels of aP2, CD36 and FAS in the liver (Fig. 7e), and PPARγ, aP2, CD36, FAS, LPL and Acetyl-CoA carboxylase (ACC) in WAT (Fig. 7f) were significantly decreased with the PPT treatment. Moreover, PPT reduced the expression of the inflammatory mediators IL-1β, IL-10, IFN-γ, iNOS and CD68 in the adipose tissue of DIO mice, whereas the expression of IL-4, IL-6 and TNF-α was not altered (Fig. 7g), indicating that adipose tissue inflammation was ameliorated. Taken together, these data above suggest that PPT regulates metabolic and inflammatory gene
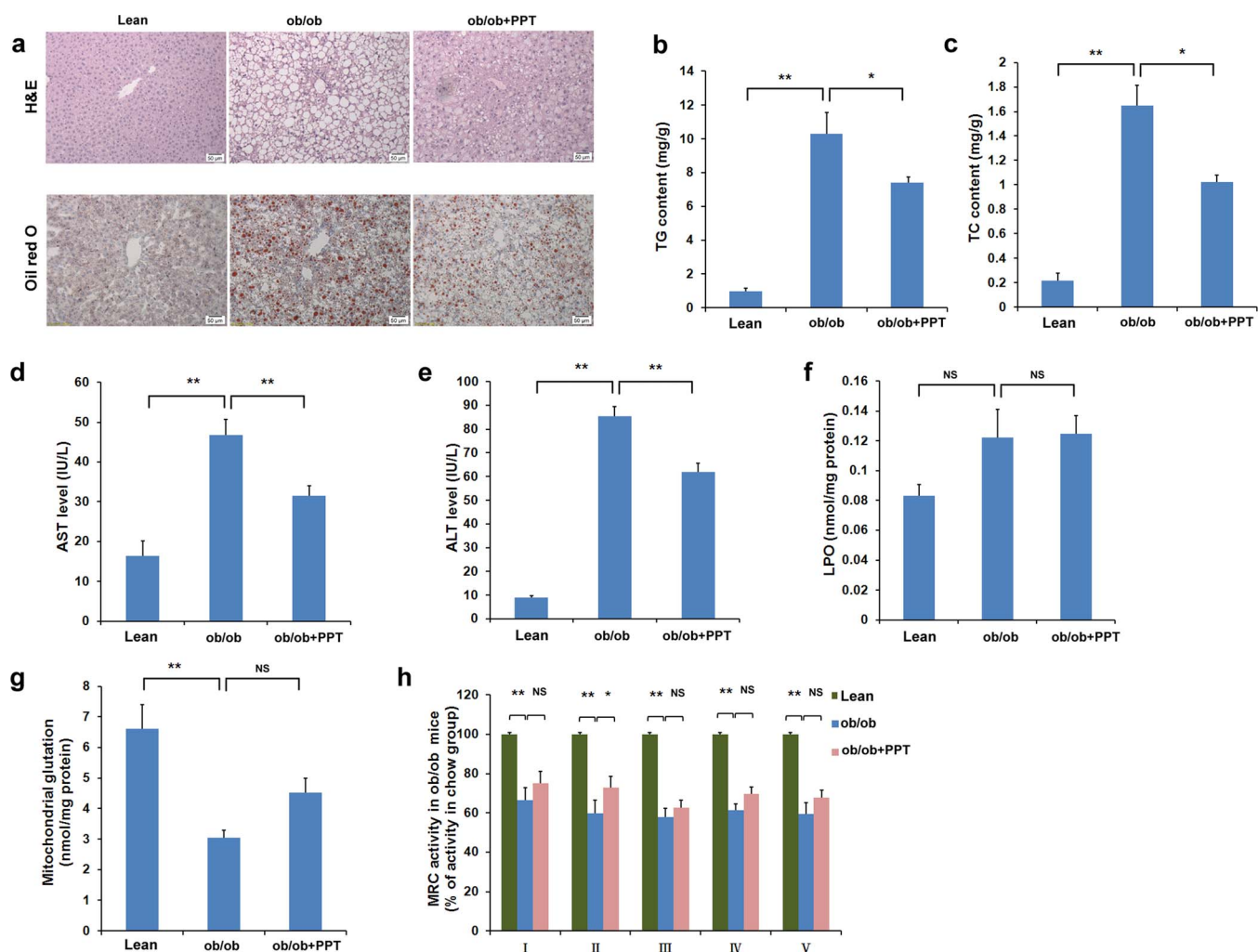
Figure 5 | **PPT ameliorates hepatic steatosis in *ob/ob* mice.** (a) H&E and Oil red O staining of liver sections (×200). (b) Liver TG level. (c) Liver TC level. (d) Serum AST level. (e) Serum ALT level. (f) Liver LPO content. (g) Liver glutathione content. (h) Mitochondrial respiratory chain level. Data are presented as means ± SEM (n = 8). *$P < 0.05$, **$P < 0.01$ vs. *ob/ob* mice.

expression *in vivo*, which may further improve insulin resistance, dyslipidemia and steatosis.

Discussion

Ginseng has been used in the treatment of obesity in traditional medicine. However, the active constituent and the mechanism of action are largely unknown. The present study demonstrates that PPT, a major monoglucoside of Rg1 ginseng ginsenosides, inhibits the adipocyte differentiation of 3T3-L1 cells. PPT alleviates metabolic disorders through the inhibition of PPARγ signaling in both DIO mice and *ob/ob* mice. Moreover, our data support that most likely, PPT is a specific ligand of PPARγ with antagonizing activity.

Numerous bioactivities have been reported for ginseng, which may contribute to the health-promoting effects as well as therapeutic effects. More than 30 ginsenosides have been purified from ginseng. They are divided into three types: protopanaxadiol (PPD)-type (Rb1, Rb2, Rb3, Rc, Rd, F2, Rg3, and Rh2), protopanaxatriol (PPT)-type (Re, Rg1, Rg2, Rg4, Rh1, and Rh4), and oleanonic acid-type saponins (Ro). The main ginsenosides in the ginseng are the ginsenosides Rb1, Rb2, Rc, Rd, Re, Rf, and Rg1[3]. Ginseng has been used to cure the obesity and diabetes in Asian. Using the 3T3-L1 adipocyte differentiation model, our study as well as others provide the primary evidence that PPT and PPT-type ginsenosides Re and Rg1 showed inhibitory effects on the differentiation of 3T3-L1 adipocytes, while PPD type ginsenosides Rb2, Rb3 and Rc displayed promotion activity

(Table 1). PPT is a major secondary metabolites of PPT-type ginsenosides, thus PPT may be responsible for the variety of biological functions of ginseng.

PPARγ is a crucial regulator of glucose and lipid homeostasis and an important pharmacological target for combating metabolic diseases. PPARγ agonists are strong insulin-sensitizing agents. However, over-activation of PPARγ can lead to serious side effects including weight gain and steatosis. On the other hand, PPARγ antagonists may inhibit lipogenesis and adipocyte differentiation, reduce fat weight and improve insulin resistance in the obese mouse. Several lines of evidence presented here supports the notion that PPT is a novel PPARγ antagonist. First, a reporter assay using a PPARγ-driven luciferase reporter showed that PPT selectively inhibited the transactivity of PPARγ induced by rosiglitazone (Fig. 6a), but not that of PPARα, PPARβ/δ and LXRα and β (Fig. 6b&c, and data not shown). This is a favorable profile of action since the inhibition of PPARα, β/δ or LXRα/β may have unwanted side effects. Second, the binding assay showed that PPT competes with rosiglitazone to bind to the human PPARγ receptor with a Ki of 3.07 μM (Fig. 6d). Third, molecular docking studies suggested PPT may interact with the ligand binding domain of PPARγ, where hydrogen bonds at Cys285, His449 and Met364 are predicted to be formed, in addition to extensive hydrophobic interactions (Fig. 6e and 6f). The predicted binding mode revealed that the interactions between PPT and the PPARγ ligand binding site mimics the observations between PPARγ
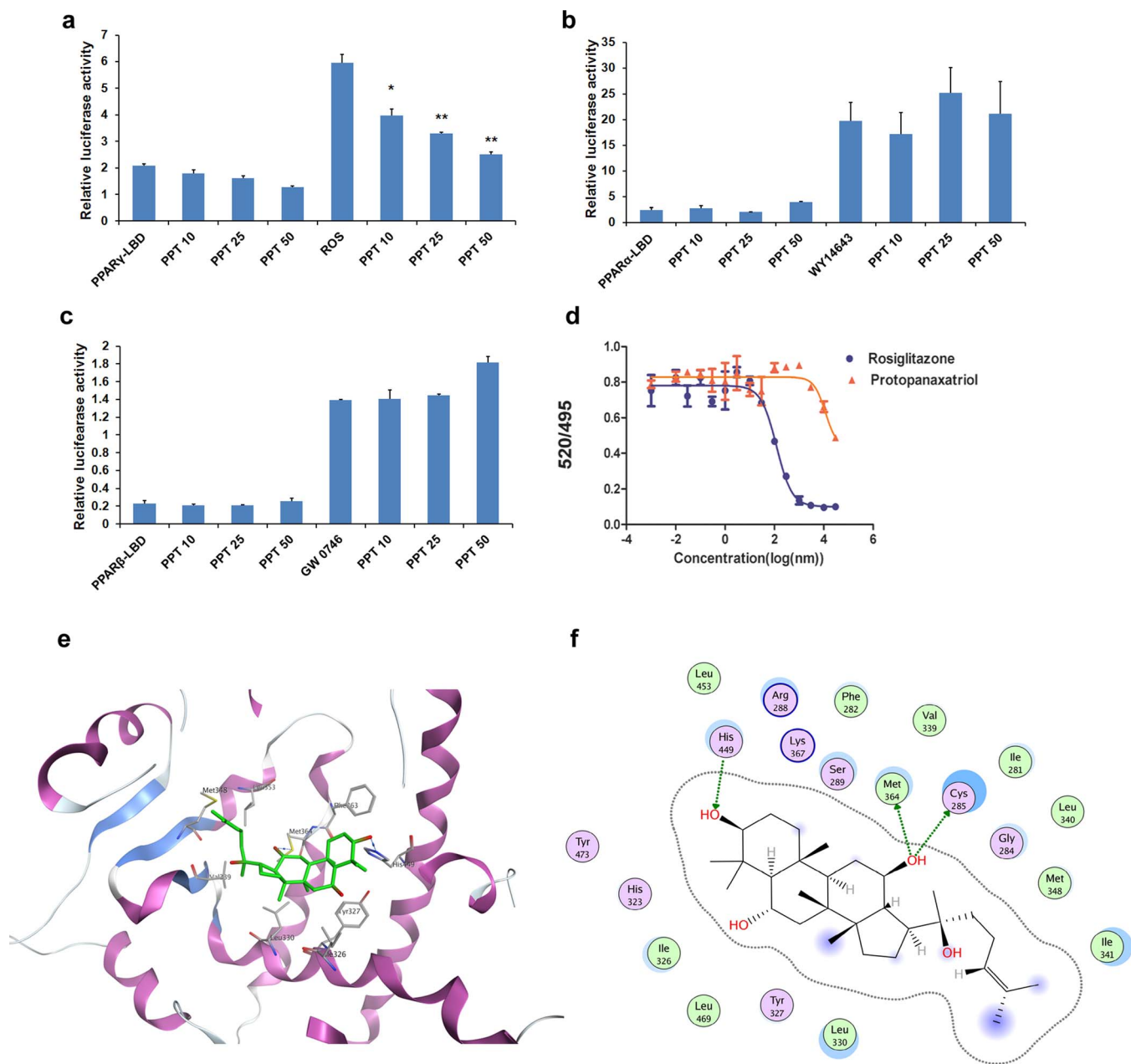
Figure 6 | PPT is a natural antagonist of PPARγ. (a)-(c). PPT specially inhibits the transcription activity of PPARγ (a), but not PPARα (b) and PPARβ (c) PPT 10, PPT 25, PPT 50: 10, 25 and 50 μM PPT. The concentration of Rosiglitazone, WY14643 and GW0742 is 10 μM. (d) Binding of PPT on PPARγ-LBD in competition with rosiglitazone in a competitive TR-FRET assay. (e) The structure of the complex of the PPARγ LBD and PPT by molecular docking. (f) The 2D- interaction map of the complex of the PPARγ LBD and PPT. Data are presented as means ± SEM (n = 3). *$P<0.05$, **$P<0.01$vs. agonist group.

and its known agonists, which suggests that PPT functions as a ligand of PPARγ. Last, PPT inhibits adipocyte differentiation of 3T3-L1 cells supported by rosiglitazone, accompanying with the reduced expression of PPARγ and its downstream genes *in vitro*. The similar effects on the expression of PPARγ and its target genes are further confirmed in both DIO mouse and *ob/ob* mouse models. Thus, most likely, PPT is a PPARγ antagonist.

PPARγ agonists may increase the number of newly differentiated small adipocytes with a concomitant reduction of large adipocytes that cause insulin resistance in part via the secretion of large amounts of TNFα and free fatty acid[41]. Heterozygous PPARγ-deficient mice were protected from the development of insulin resistance under a HF diet, because the presence of more small adipocytes led to a reduction in the secretion of these molecules[41]. Moreover, in humans,

it has been reported that the Pro12Ala mutation in the PPARγ2 gene decreases PPARγ activity, and individuals with this mutation have a lower body mass index and increased insulin sensitivity[42,43]. Thus, the deficiency of PPARγ appears to protect obesity and insulin resistance. The identification of PPARγ antagonists such as PPT may provide potential novel therapeutic approaches for obesity and obesity-linked insulin resistance.

In principle, protection of weight gain and adipocyte hypertrophy can be achieved by either reduced food intake or increased energy expenditure, or a combination of both. In the PPT-treated DIO mouse, food intake was not significantly reduced (Fig. 2c) and energy expenditure was increased (Fig. 2e). These results were similar to those observed in PPARγ$^{+/-}$ mice[1]. Interestingly PPT treatment also significantly decreased leptin levels in DIO mice (Fig. 2j), suggesting
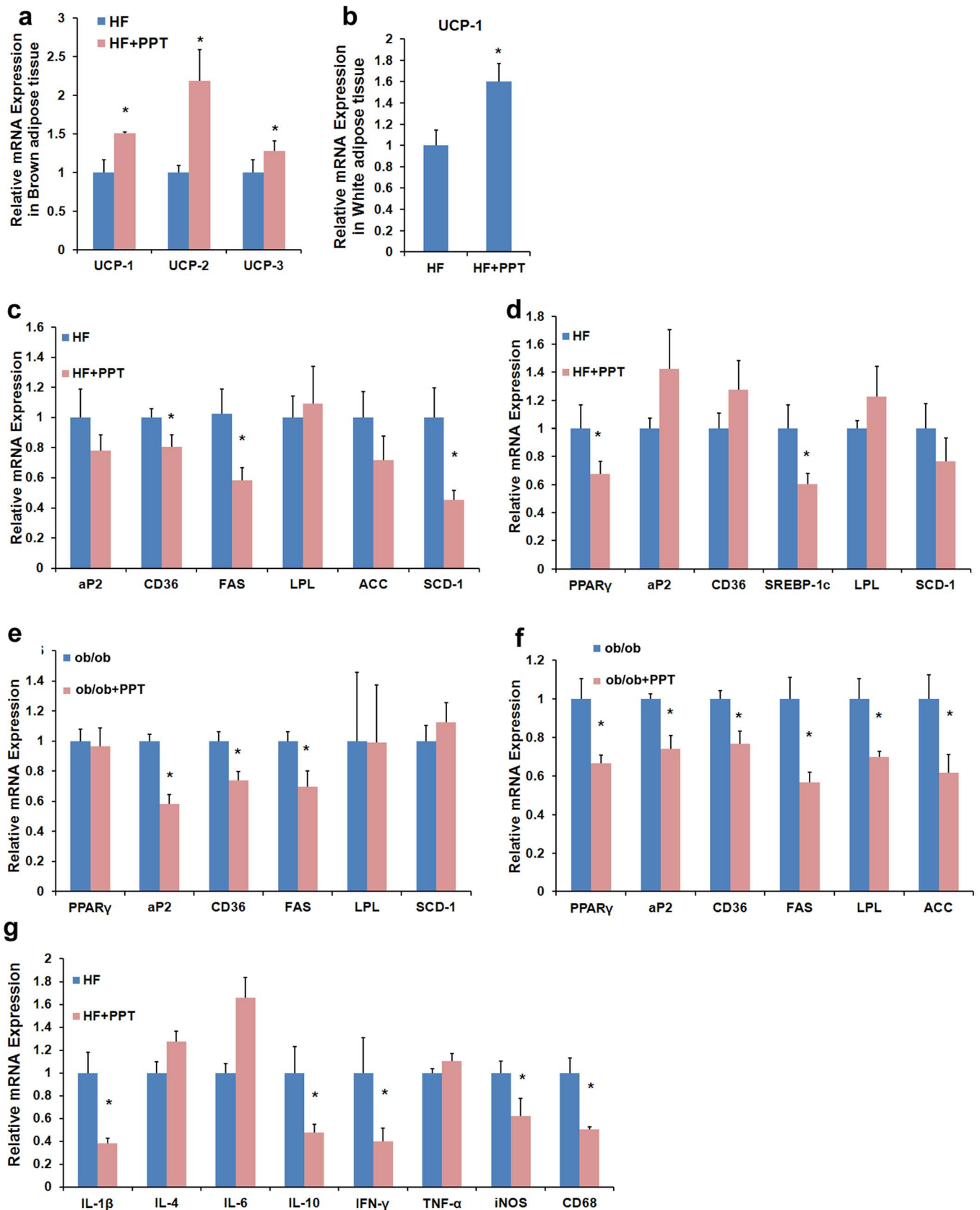
Figure 7 | PPT inhibits the mRNA expression of the PPARγ target genes. (a) The mRNA expression level of the thermogenic genes in BAT in DIO mice. (b) The mRNA expression level of the UCP-1 in WAT of DIO mice. (c)- (d) RT-PCR analysis of gene expression in liver tissue (b) and WAT (c) of DIO mice (n = 6). (e)- (f) RT-PCR analysis of gene expression in liver tissue (e) and WAT (f) of *ob/ob* mice (n = 6). (g) The mRNA expression level of the inflammatory genes in WAT of DIO mice. Data are presented as means ± SEM (n = 6). *$P<0.05$, **$P<0.01$vs. *ob/ob* mice.

that PPT may improve the leptin resistance caused by the high-fat diet. Probably, the reduced leptin level is due to more small adipocytes and lower adipose tissue mass in the PPT-treated DIO mice (Fig. 2). However, in leptin deficiency *ob/ob* mice, PPT did not improved obesity, indicating that the intact leptin signaling may play a role in the weight-reducing effect of PPARγ antagonists. Nevertheless, our data cannot exclude other possibilities, such as that PPT may influence the leptin level through insulin related mechanisms.

The lesions of NAFLD are revealed in the liver of all DIO mice. The improved liver morphology, the decreased fat droplets, as well as the attenuated steatosis, were observed in all PPT-treated DIO mice (Fig. 3a). Previous studies have demonstrated that the inhibition or deletion of PPARγ may significantly ameliorate liver histology in obese mice. In sharp contrast, the activation of PPARγ by its agonist exhibited a marked increase in severe microvesicular steatosis[44], exacerbated hepatic steatosis, and increased hepatic triglycerides correlated with hepatic PPARγ expression[45]. Our data both *in vitro* and *in vivo* show that PPT could inhibit the expression of PPARγ and its downstream genes (Fig. 7), indicating that PPT might improve hepatic steatosis by inhibiting PPARγ signaling.

Oxidative stress and abnormal MRC level are involved in the pathogenesis of hepatic steatosis. The PPARγ agonists, such as rosiglitazone and pioglitazone, have been reported to reduce MRC complexes and increase oxidative stress, which exacerbate liver steatosis[19]. Administration of PPT in DIO mice and *ob/ob* mice led to a marked increase of the MRC complexes, particularly of complexes I and IV, in DIO mice, and complex II in *ob/ob* mice. In addition, PPT treatment decreased the expression of PPARγ target genes in the mouse liver, suggesting that PPT may improve steatosis through the inhibition of PPARγ activity and the MRC levels in the liver of obese mouse.

Obesity is associated with a low-grade inflammation in white adipose tissue and liver, which may exacerbate insulin resistance, steatosis and diabetes. Control of inflammation seems important in the clinic treatment of the metabolic diseases. PPT reduced the serum IL-1β (Fig. 3i), as well as IL-10, IFN-γ, iNOS and CD68 mRNA in WAT of DIO mice (Fig. 7g). Therefore, PPT may ameliorate the inflammation state in obese mice, and it could be the part of mechanism for the improvement of metabolic disorders by PPT.

In conclusion, we identified PPT as a novel, natural antagonist of PPARγ. PPT is able to improve insulin resistance, reduce body weight, and ameliorate hepatic steatosis in both DIO mice and *ob/ob* mice. Our data suggest that PPT may be developed as a novel therapy or dietary supplement for obesity and obesity-linked steatosis.

Methods

Cell culture. 3T3-L1 pre-adipocytes were maintained in DMEM supplemented with 10% fetal bovine serum (FBS, Hyclone, Logan, UT, USA). The cells were grown in 12- or 24-well plates to full confluence for 2 days and differentiation was induced in DMEM supplemented with 10% FBS and 1 μM dexamethasone (DEX, Sigma-Aldrich, St. Louis, MO, USA)/10 μg/ml insulin (Sigma-Aldrich, St. Louis, MO, USA)/ 10 μM Rosiglitazone (ROS. Sigma-Aldrich, St. Louis, MO, USA). After 48 h, the medium was changed with only the addition of insulin for an additional 2 days. Thereafter, the medium was replenished with DMEM with 10% FBS for differentiation at 37°C, in a 7.5% CO₂ atmosphere. During the induction, PPT was added to the medium at the beginning of induction of 3T3-L1 cells to observe its effects on 3T3-L1 adipocyte differentiation. PPT was used at different times of differentiation at a concentration of 50 μM. At RT-PCR experiment, cells were treated with PPT and differentiation medium after confluence for 2 days and 8 days and concentration is 50 μM.

For screening, we used differentiation medium (DM) containing 10 μg/ml insulin, 0.5 μM dexamethasone and 0.8 mM isobutylmethyl xanthine (IBMX, Sigma, St. Louis, MO, USA). The other methods are the same as the above. HEK293T cells were cultured in DMEM with 10% FBS and a 5% CO₂ atmosphere. All compounds were reconstituted in DMSO and added to the medium at the indicated concentration.

Oil red staining. On day 6, 3T3-L1 adipocytes were washed twice with phosphate-buffer saline (PBS) and then fixed with 10% formalin for 10 min. Lipogenesis was determined by the staining of lipids with Oil Red O (Sigma-Aldrich, St. Louis, MO, USA) for 30 min at 50°C. Pictures were taken using an Olympus (Tokyo, Japan) microscope.

Animals and diets. All experiments were carried out according to the guidelines and the regulations of the Ethical Committee of Shanghai University of Traditional Chinese Medicine. The protocols were approved by the Institute Animal Care and Use Committee of Shanghai University of Traditional Chinese Medicine. Female C57BL/6 mice were purchased from SLAC Laboratory (Shanghai, China) at 7 weeks of age. The mice were placed on a high-fat diet (60% of calories derived from fat, 5.24 Kcal/gm, Research Diets, New Brunswick, NJ, USA, D12492) for 3 months to induce obesity and then the obese mice were randomly divided into two groups (n = 8). High-fat control mice (HF) were kept on the HF diet, while PPT was mixed into the diet at 0.1 g/100 g (W/W). The lean control mice (Chow) were placed on a low-calorie diet (Chow diet) (10% of calories derived from fat, 3.85 Kcal/gm, Research Diets, D12450B). The body weight and food intake amount were recorded in both treated groups and controls.

The C57BL/KsJ-*ob/ob* mice were purchased from Animal Center, Nanjing University (Nanjing, China). Eleven week-old *ob/ob* mice were dosed each day with PPT (100 mg kg⁻¹ day⁻¹) using oral gavage in a water vehicle. Control mice were given water with oral gavage for 2 weeks.

Glucose tolerance and insulin tolerance tests. The intraperitoneal glucose tolerance test (IPGTT) was performed after 12 h of fasting and intraperitoneal insulin tolerance tests (IPITT) applied blood glucose levels of non-fasted mice. Glucose levels were determined from the tail vein (0 min) before the injection of glucose and insulin (Sigma, St. Louis, MO, USA). Additional blood samples were collected at regular intervals (15, 30, 60, 90 and 120 min) for glucose measurements following the injection of glucose (1 g/kg body weight) and insulin (0.75 U/kg body weight).

Biochemistry analysis. At the end of the treatment, overnight fasting blood samples were withdrawn by cardiac puncture after anesthesia (Urethane, 20%, w/v). The blood samples were centrifuged at 3000 rpm for 15 min to separate serum from the samples. Serum triglyceride (TG), total cholesterol (TC), high-density lipoprotein-cholesterol (HDL-c) and low-density lipoprotein-cholesterol (LDL-c) levels were examined by an automatic analyzer (Hitachi 7020, Tokyo, Japan) using 100 μl of heart blood serum. Free fatty acid (FFA) was measured by microplate reader at 570 nm using 10 μl of heart blood serum according to the instructions from the manufacturers. The kit for FFA was obtained from BioAssay System (BioAssay, CA, USA).

Rectal temperature Measurement. The rectal temperature of mice was examined with a rectal probe attached to a digital thermometer (Physitemp, NJ, USA). At room temperature, the body temperature of the mice was measured using a rectal probe.

Scanning Electron Microscope. The adipose tissue was fixed in 1% osmium tetraoxide. The images were taken using A Philips XL-30 scanning electron microscope.

HE staining and oil red O staining. For H&E staining, the tissue was fixed in 10% formaldehyde, embedded in paraffin and cut into 10 μm sections according to a standard protocol. The sections were stained with hematoxylin and eosin. The 3T3-L1 adipocytes or frozen sections of liver were washed with PBS twice, fixed with 10% formalin at room temperature for 10 minutes, and then stained with oil red O (Sigma-Aldrich, St. Louis, MO, USA) at 60°C for 10 minutes. Pictures were then taken using an Olympus (Tokyo, Japan) microscope.

Live content analysis. The liver tissues were weighed and homogenized in tissue lysis buffer (20 mM Tris·HCl pH 7.5, 150 mM NaCl, 1% Triton) and extracted with an equal volume of chloroform. The chloroform layers were dried and dissolved with isopropyl alcohol to measure TG and TC levels according to the manufacturer's instructions (KINGHA WK, China).

Enzyme-Linked ImmunoSorbent Assay (ELISA). Serum insulin, leptin, adiponectin, IL-1β and IL-6 levels were measured using enzyme-linked immunosorbent assay according the instructions from the manufacturers. The mouse serum was stored at −80°C and incubated at 37°C for thawing prior to analysis. The kits for insulin, leptin and adiponectin were obtained from ALPCO Diagnostics (Salem, NH, USA), R&D Systems (Oxon, UK) and AdipoGen (Seoul, Korea), respectively. The kits for IL-1β and IL-6 were purchased from eBioscience (San Diego, CA, USA).

For mitochondrial respiratory chain level assays, frozen liver tissues (50–70 mg) were homogenized with 9 volumes cold saline, and centrifuged at 2500 rpm for 10 min. Enzyme levels in supernatants were measured according the instructions from the manufacturer (Shanghai Bioye Biotechnology Co., Ltd, China). Briefly, 10 μl of sample was incubated with HRP-labeled antibodies against the complexes at 30°C for 30 min. TMB (3,3′,5,5′-Tetramethylbenzidine) was used to develop color. Respiratory chain enzymes were measure in microplate reader (Synergy HT, BioTek, USA) and examined the absorbance at 450 nm. Activity was normalized using liver weight.

Table 2 | Sequences of the primers used in real time PCR

Gene	Forward primer	Reverse primer
β-Actin	TGTCCACCTTCCAGCAGATGT	AGCTCAGTAACAGTCCGCCTAGA
FAS	CTGAGATCCCAGCACTTCTTGA	GCCTCCGAAGCCAAATGAG
LPL	ATCGGAGAACTGCTCATGATGA	CGGATCCTCTCGATGACGAA
C/EBP-α	CGCAAGAGCCGAGATAAAGC	CACGGCTCAGCTGTTCCA
C/EBP-β	GGGGTTGTTGATGTTTTTGG	CGAAACGGAAAAGGTTCTCA
αP2	CATGGCCAAGCCCAACAT	CGCCCAGTTTGAAGGAAATC
ACC	GAATCCTCTGGTGACAATGCTTATT	GGTCTTGCTGAGTTGGGTTAGCT
CD36	GCTTGCAACTGTCAGCACAT	GCCTTGCTGTAGCCAAGAAC
PPARγ	TGCTGTATTTGAATCCGACGTT	GCTCTTTAGAAACTCCCTTGTCATG
SREBP-1c	GGCTATTCCGTGAACATCTCCTA	ATCCAAGGGCAGTTCTTGTG
UCP-1	CATCACCACCCTGGCAAAA	AGCTGATTTGCCTCTGAATGC
UCP-2	GGGCACTGCAAGCATGTGTA	TCAGATTCCTGGGCAAGTCACT
UCP-3	TGGCCCAACATCACAAGAAA	TCCAGCAACTTCTCCTTGATGA
SCD-1	TCACCTTGAGAGAAGAATTAGCA	TTCCCATTCCCTTCACTCTGA
IL-1β	TCGTGCTGTCGGACCCATAT	GGTTCTCCTTGTACAAAGCTCATG
IL-4	GCAGAGACTCTTTCGGGCTTT	CATTCATGGTGCAGCTTATCGA
IL-6	AACCACGGGCTTCCCTACTT	TCTGTTGGGAGTGGTATCCTCTGT
IL-10	GCCAAGCCTTATCGGAAATG	CTTGATTTCTGGGCCATGCT
TNF-α	ATGGATCTCAAAGACAACCAACTAG	ACGGCAGAGAGGAGGTTGACTT
iNOS	CTTGGAGCGAGTTGTGGATTGTC	TAGGTGAGGGCTTGGCTGAGTG
IFN-γ	CTGAGACAATGAACGCTACACACT	CTTTTCTTCCACATCTATGCCACTT
CD68	TCACCTTGACCTGCTCTCTCTAA	GCTGGTAGGTTGATTGTCGTCTG

Quantitative real-time PCR. Total RNA was extracted from the liver and adipose tissue of mice using TRIzol reagent (TaKaRa, Shiga, Japan) according to the manufacturer's instructions[46]. The first strand cDNA was synthesized using a cDNA synthesis kit (Fermentas, Madison, WI, USA), and gene expression levels were analyzed by quantitative real-time RT-PCR using the ABI StepOnePlus Real Time PCR system (Applied Biosystems, Grand Island, NY, USA). Samples were incubated for an initial denaturation at 95°C for 10 min, followed by 40 PCR cycles each consisting of 95°C for 15 s and 60°C for 60 s. The primers used in the experiments are shown in Table 2. The mRNA levels of all genes were normalized using β-actin as an internal control.

Luciferase reporter assays. The plasmids pCMX-Gal-mPPAR α,β, γ LBD, pCMX-Gal, and the Gal4 reporter vector MH100-4-TK-Luc were obtained from Dr. R Evants. HEK293T cells were plated in 48-well plates in 250 μl of DMEM with 10% FBS. The next day, cells were co-transfected with PPAR and LXR expression plasmids and their reporter construct using FuGENE-HD (Roche, Switzerland). One day later, compounds were added to the medium. After 24 h treatment, cells were lysed and harvested for the determination of luciferase activity. The luciferase reporter assays were carried out using the Dual-Luciferase Reporter Assay System (Promega, Madison, WI, USA). Firefly luciferase value was normalized to renilla luciferase. All of the experiments were performed in duplicate and repeated at least three times independently.

Time-Resolved Fluorescence Resonance Energy Transfer (TR-FRET). The nuclear receptor competitive binding assay was used to identify PPARγ ligands based on time-resolved fluorescence resonance energy transfer (TR-FRET) according to the manufacturer's protocol (Lanthascreen, Invitrogen, Darmstadt, Germany). Briefly, when a fluorescent ligand (tracer) is bound to the receptor (the conjugate of antibody and nuclear receptor protein), energy transfer from the antibody to the tracer occurs, and a high 520/495 ratio is detected. A compound under test displaces the tracer from PPARγ-LBD, which leads to a decrease in the FRET signal and the observation of a low TR-FRET ratio. The tracer and receptor/antibody mixture was incubated for 1 hour. IC50 was gained using GraphPad Prism 5.0 and Ki was calculated according to equation: Ki = IC50/(1+ [tracer]/KD). The calculation was performed by applying the Cheng and Prusoff equation[47].

Docking study. Before docking, the three-dimensional structure of human PPARγ was prepared. Based on the superposed structure, 2I4J was chosen as the start of the docking simulation because of the higher resolution. The PPT was built with Molecule Builder in MOE and its conformation was generated using Conformational Search and Saturation Ring Search in MOE. Moreover, the conformation as a ligand was submitted to the docking module in MOE. Classical Triangle Matching was chosen as the placement method and the force-field was employed as the refinement method for pose refinement. The receptor-ligand affinity was calculated by London dG and GBVI/WAS dG score. The reasonable binding models were analyzed in MOE.

Determination of hepatic lipid peroxides content and glutathione content. For the determination of total lipid peroxides, 70 mg of liver was 10× homogenized in saline and centrifuged at 2500 rpm for minutes. Lipid peroxide content was measured in 200 μl of supernatant according to the manufacturer's protocol (Jiancheng Bioengineering Institute, Nanjing, China). The kit for glutathione determination was purchased from Beyotime Biotechnology. The protein content of supernatants was determined using the Bicinchoninic Acid assay (Beyotime Biotechnology, Shanghai, China).

Statistical analysis. Data are expressed as means ± SE. Data analyses were performed using the SPSS15.0 for Windows statistical program. Paired or unpaired two tailed t-tests were used to detect two groups difference or among more than two groups using analysis of variance (ANOVA) followed by post-hoc test with LSD test. Differences were regarded as significant when $P < 0.05$.

1. Kubota, N. et al. PPAR gamma mediates high-fat diet-induced adipocyte hypertrophy and insulin resistance. Mol Cell **4**, 597–609 (1999).
2. Bugyi, B. From the history of the discovery of radioactivity (Henri Becquerel). Orvosi Hetilap **114**, 3099–3100 (1973).
3. Cheng, Y. & Prusoff, W. H. Relationship between the inhibition constant (K1) and the concentration of inhibitor which causes 50 per cent inhibition (I50) of an enzymatic reaction. Biochem Pharmacol **22**, 3099–3108 (1973).
4. Blume, A. J., Dalton, C. & Sheppard, H. Adenosine-mediated elevation of cyclic 3':5'-adenosine monophosphate concentrations in cultured mouse neuroblastoma cells. Proc Natl Acad Sci USA **70**, 3099–3102 (1973).
5. Yang, W. et al. The effects of periconceptional risk factor exposure and micronutrient supplementation on birth defects in Shaanxi Province in Western China. PLoS One **7**, e53429 (2012).
6. Miles, P. D., Barak, Y., He, W., Evans, R. M. & Olefsky, J. M. Improved insulin-sensitivity in mice heterozygous for PPAR-gamma deficiency. J Clin Invest **105**, 287–292 (2000).
7. Yamauchi, T. et al Inhibition of RXR and PPARgamma ameliorates diet-induced obesity and type 2 diabetes. J Clin Invest **108**, 1001–1013 (2001).
8. Matsusue, K. et al. Liver-specific disruption of PPARgamma in leptin-deficient mice improves fatty liver but aggravates diabetic phenotypes. J Clin Invest **111**, 737–747 (2003).
9. Gong, Z. et al The role of tanshinone IIA in the treatment of obesity through peroxisome proliferator-activated receptor gamma antagonism. Endocrinology **150**, 104–113 (2009).
10. Zhang, Y. et al Rhein Reduces Fat Weight in db/db Mouse and Prevents Diet-Induced Obesity in C57Bl/6 Mouse through the Inhibition of PPARgamma Signaling. PPAR Res **2012**, 374936 (2012).
11. Goto, T., Kim, Y. I., Takahashi, N. & Kawada, T. Natural compounds regulate energy metabolism by the modulating the activity of lipid-sensing nuclear receptors. Mol Nutr Food Res **57**, 20–33 (2013).
12. Browning, J. D. et al Prevalence of hepatic steatosis in an urban population in the United States: impact of ethnicity. Hepatology **40**, 1387–1395 (2004).
13. Yki-Jarvinen, H. Fat in the liver and insulin resistance. Ann Med **37**, 347–356 (2005).
14. Milic, S. & Stimac, D. Nonalcoholic fatty liver disease/steatohepatitis: epidemiology, pathogenesis, clinical presentation and treatment. Dig Dis **30**, 158–162 (2012).
15. Yu, S. et al. Adipocyte-specific gene expression and adipogenic steatosis in the mouse liver due to peroxisome proliferator-activated receptor gamma1 (PPARgamma1) overexpression. J Biol Chem **278**, 498–505 (2003).

16. Uno, K. *et al.* Neuronal pathway from the liver modulates energy expenditure and systemic insulin sensitivity. *Science* **312**, 1656–1659 (2006).

17. Inoue, M. *et al.* Increased expression of PPARgamma in high fat diet-induced liver steatosis in mice. *Biochem Biophys Res Commun* **336**, 215–222 (2005).

18. Rull, A. *et al.* Rosiglitazone and Fenofibrate Exacerbate Liver Steatosis in a Mouse Model of Obesity and Hyperlipidemia. A Transcriptomic and Metabolomic Study. *J Proteome Res*, (2014).

19. Garcia-Ruiz, I. *et al.* Effects of rosiglitazone on the liver histology and mitochondrial function in ob/ob mice. *Hepatology* **46**, 414–423 (2007).

20. Gavrilova, O. *et al.* Liver peroxisome proliferator-activated receptor gamma contributes to hepatic steatosis, triglyceride clearance, and regulation of body fat mass. *J Biol Chem* **278**, 34268–34276 (2003).

21. Moran-Salvador, E. *et al.* Role for PPARgamma in obesity-induced hepatic steatosis as determined by hepatocyte- and macrophage-specific conditional knockouts. *FASEB J* **25**, 2538–2550 (2011).

22. Jeon, W. J., Oh, J. S., Park, M. S. & Ji, G. E. Anti-hyperglycemic effect of fermented ginseng in type 2 diabetes mellitus mouse model. *Phytother Res* **27**, 166–172 (2013).

23. Attele, A. S. *et al.* Antidiabetic effects of Panax ginseng berry extract and the identification of an effective component. *Diabetes* **51**, 1851–1858 (2002).

24. Liu, Z. *et al.* Antidiabetic effects of malonyl ginsenosides from Panax ginseng on type 2 diabetic rats induced by high-fat diet and streptozotocin. *J Ethnopharmacol* **145**, 233–240 (2013).

25. Cho, W. C. *et al.* Ginsenoside Re of Panax ginseng possesses significant antioxidant and antihyperlipidemic efficacies in streptozotocin-induced diabetic rats. *Eur J Pharmacol* **550**, 173–179 (2006).

26. Sotaniemi, E. A., Haapakoski, E. & Rautio, A. Ginseng therapy in non-insulin-dependent diabetic patients. *Diabetes Care* **18**, 1373–1375 (1995).

27. Lee, M. R. *et al.* Anti-obesity effects of black ginseng extract in high fat diet-fed mice. *J Ginseng Res* **37**, 308–349 (2013).

28. Gu, W., Kim, K. A. & Kim, D. H. Ginsenoside Rh1 ameliorates high fat diet-induced obesity in mice by inhibiting adipocyte differentiation. *Biol Pharm Bull* **36**, 102–107 (2013).

29. Lee, H., Park, D. & Yoon, M. Korean red ginseng (Panax ginseng) prevents obesity by inhibiting angiogenesis in high fat diet-induced obese C57BL/6J mice. *Food Chem Toxicol* **53**, 402–408 (2013).

30. Hwang, J. T. *et al.* Antiobesity effect of ginsenoside Rg3 involves the AMPK and PPAR-gamma signal pathways. *Phytother Res* **23**, 262–266 (2009).

31. Qi, L. W. *et al.* Metabolism of ginseng and its interactions with drugs. *Curr Drug Metab* **12**, 818–822 (2011).

32. Korivi, M. *et al.* Ginsenoside-Rg1 Protects the Liver against Exhaustive Exercise-Induced Oxidative Stress in Rats. *Evid Based Complement Alternat Med* **2012**, 932165 (2012).

33. Rangwala, S. M. & Lazar, M. A. Transcriptional control of adipogenesis. *Annu Rev Nutr* **20**, 535–559 (2000).

34. Rosen, E. D. & Spiegelman, B. M. Molecular regulation of adipogenesis. *Annu Rev Cell Dev Biol* **16**, 145–171 (2000).

35. Schinner, S., Scherbaum, W. A., Bornstein, S. R. & Barthel, A. Molecular mechanisms of insulin resistance. *Diabet Med* **22**, 674–682 (2005).

36. Koyama, K., Chen, G., Lee, Y. & Unger, R. H. Tissue triglycerides, insulin resistance, and insulin production: implications for hyperinsulinemia of obesity. *Am J Physiol* **273**, E708–713 (1997).

37. Despres, J. P. *et al.* Hyperinsulinemia as an independent risk factor for ischemic heart disease. *N Engl J Med* **334**, 952–957 (1996).

38. Ren, J. Leptin and hyperleptinemia - from friend to foe for cardiovascular function. *J Endocrinol* **181**, 1–10 (2004).

39. Ebbert, J. O. & Jensen, M. D. Fat depots, free fatty acids, and dyslipidemia. *Nutrients* **5**, 498–508 (2013).

40. Nedergaard, J. & Cannon, B. The Browning of White Adipose Tissue: Some Burning Issues. *Cell Metab* **20**, 396–407 (2014).

41. Okuno, A. *et al.* Troglitazone increases the number of small adipocytes without the change of white adipose tissue mass in obese Zucker rats. *J Clin Invest* **101**, 1354–1361 (1998).

42. Deeb, S. S. *et al.* A Pro12Ala substitution in PPARgamma2 associated with decreased receptor activity, lower body mass index and improved insulin sensitivity. *Nat Genet* **20**, 284–287 (1998).

43. Kadowaki, T. *et al.* The role of PPARgamma in high-fat diet-induced obesity and insulin resistance. *J Diabetes Complications* **16**, 41–45 (2002).

44. Bedoucha, M., Atzpodien, E. & Boelsterli, U. A. Diabetic KKAy mice exhibit increased hepatic PPARgamma1 gene expression and develop hepatic steatosis upon chronic treatment with antidiabetic thiazolidinediones. *J Hepatol* **35**, 17–23 (2001).

45. Watkins, S. M., Reifsnyder, P. R., Pan, H. J., German, J. B. & Leiter, E. H. Lipid metabolome-wide effects of the PPARgamma agonist rosiglitazone. *J Lipid Res* **43**, 1809–1817 (2002).

46. Hummon, A. B., Lim, S. R., Difilippantonio, M. J. & Ried, T. Isolation and solubilization of proteins after TRIzol extraction of RNA and DNA from patient material following prolonged storage. *Biotechniques* **42**, 467–470, 472 (2007).

47. Chang, Y. & Prusoff, W. Relationship between the inhibition constant (Ki) and the concentration of inhibitor which causes 50 percent inhibitions (I50) of on enzymatic reaction. *Biochem Pharmacol* **22**, 3099–3108 (1973).

Author contributions

Additional information